JOURNAL OF OPTOELECTRONICS AND ADVANCED MATERIALS Vol. 9, No. 12, December 2007, p. 3939 - 3945

Lidar-calibrated regional models for satellite retrieval of primary productivity in the Southern Ocean

L. FIORANI*, I. G. OKLADNIKOV[a], A. PALUCCI
ENEA, FIM-FISLAS, Via Fermi 45, 00044 Frascati RM, Italy
[a]IMCES, SCERT, Akademicheskii Avenue 10/3, 634055 Tomsk, Russia

Although there is experimental evidence on climate change, the debate on its causes is still open. It is certain that oceanic phytoplankton is a major sink for carbon dioxide. Conversely, a clear understanding of the role played by cold regions in this hot problem needs more investigations. For instance, the chemico-physical dynamics of the Southern Ocean define oceanographic provinces where endemic phytoplankton develops and satellite algorithms should be locally calibrated in order to provide accurate estimates of carbon fixation or primary productivity. As a contribution to the solution of this climatic puzzle, in this study satellite algorithms are calibrated in three regions of the Ross Sea with the measurements carried out by the ENEA lidar fluorosensor. Those results show that the standard primary productivity model should be reviewed and demonstrate that the chlorophyll-a algorithm has to be locally calibrated in each oceanographic province in order to provide accurate data.

(Received May 30, 2007; accepted December 4, 2007)

Keywords: Remote sensing, Lidar fluorosensor, Satellite radiometer, Primary productivity, Regional models

1. Introduction

Mixing processes involving water masses of the Ross Sea result in the definition of oceanographic provinces [1] where the development of endemic phytoplankton is favored [2]. Recent studies demonstrate that the lack of knowledge of the taxonomic composition and of the bio-optical properties of the dominant species in an oceanographic province may result in a significant misestimate of its chlorophyll-a (Chl-a) content [3]. In particular, there is a growing convergence indicating that the Chl-a content of the Southern Ocean is underestimated by ocean color satellite radiometers [4], as in the case of the Sea-viewing Wide Field-of-view Sensor (SeaWiFS) [5]. This explains the need of in situ measurements in the oceanographic provinces of the Ross Sea, as those carried out by the ENEA lidar fluorosensor (ELF) [6], on board of the Research Vessel Italica. Moreover, if one wants to take advantage of the global coverage provided by ocean color satellite radiometers, a careful attention should be paid in atmospheric corrections [7] and calibrations/validations [8] involving in situ measurements. Usual match up analysis of satellite versus in situ Chl-a values relies in relatively few stations were seawater samples are analysed by high performance liquid chromatography (HPLC): for example, the Chl-a comparison between satellite retrievals and in situ data from the fourth SeaWiFS reprocessing is based on 262 match ups [9]. On the contrary, many lidar measurements can be compared with one satellite retrieval: ELF emits a laser pulse every 0.1 s and, as a result, acquires thousands of signals during the time taken by the ship to span a satellite pixel [10]. Moreover, while a station cover only one point of a pixel, ELF data represent a wider zone because they are distributed along a track crossing the pixel. As far as primary productivity (PP) is concerned, taking into account that Chl-a is the main variable of the vertically generalized production models [11], one should expect that the Chl-a algorithms for satellite sensors [12] require a regional calibration [13] for an accurate assessment of PP in those oceanographic provinces.

A PP calculation calibrated with ELF in the whole Ross Sea has already been described in a previous paper [14] and the interested reader will find there details and references on satellite sensors, ELF, Chl-a algorithms and PP models: here we focus only on the calibration with ELF of that PP calculation in key regions of the Ross Sea. For this purpose, a non conventional statistical technique is applied to ELF Chl-a measurements and SeaWiFS radiance data.

2. Instruments and methods

2.1 ELF

ELF [6] is part of a complete laboratory, including local and remote instruments for continuous monitoring and in situ sampling, lodged into an ISO 20' container. It is assisted by ancillary instruments: a lamp spectrofluorometer, a pulsed amplitude fluorometer, a solar radiance detector, measuring the photosynthetically available radiation (PAR), and a global positioning system.

The light source is a frequency-tripled Nd:YAG laser (355 nm) followed by a beam expander. ELF transmits the exciting pulse and receives the generated radiation through an optical window and an external mirror in order to reach the sea surface at normal incidence. The optical signal, after collection by a telescope, traverses a dichroic filter, rejecting most of the laser beam, and is forwarded by a multi-arm optical fiber to interference filters. After that spectral selection, photomultipliers perform the detection. Their electronic output is digitized by analog-to-digital converters. A personal computer, embedded in a versa

module eurocard bus, controls all the experimental settings, including the normal or pump-and-probe excitation, the laser transmitter energy, the photomultipliers high voltage and gating time and the data acquisition parameters.

The beam footprint on the sea surface is a circle of about 0.1 m. The depth of the probed layer (15 m) is determined by an electronic gate. The main spectral channels have a full width at half maximum of 5 nm and are centered at 404, 450, 585 and 680 nm, corresponding to water Raman backscattering, chromophoric dissolved organic matter (CDOM), phycoerythrin and Chl-a fluorescence, respectively.

At first, the concentrations of CDOM, phycoerythrin and Chl-a are released in Raman units (fluorescence-to-Raman ratio). The transformation from Raman units to mg m^{-3} is performed by calibration with conventional techniques in some selected points.

2.2 SeaWiFS

SeaWiFS [5] was launched on August 1, 1997 on board the OrbView-2 satellite and started data acquisition on September 4, 1997. It operates with 8 channels in the visible and near-infrared range of the electromagnetic spectrum and greatly improved our understanding of the oceanic processes as its accuracy resulted better than 35% for Chl-a concentration over the range of 0.05-50 mg m^{-3}.

Regional maps of Chl-a concentration are obtained from satellite imagery thanks to atmospheric corrections [7] and bio-optical algorithms [8]. Firstly, the water-leaving radiance is calculated with the atmospheric corrections that remove from the sensor measurements the contributions of air molecules and aerosols. Secondly, the Chl-a concentration is retrieved from the water-leaving radiances in the visible bands with a set of empirical equations named bio-optical algorithms. If the data are calibrated through in situ measurements, quantitative estimations of Chl-a concentrations are obtained within the surface layer of a given water body.

2.3 Chl-a algorithm

The ELF-calibrated SeaWiFS bio-optical algorithm [14] is based on the linear fit of the log-log plot of the ELF Chl-a concentration versus the MERIS 490-555 band ratio, i.e.:

$$\log_{10} C = a_0 + a_1 R,$$

where C is the chlorophyll-a concentration in mg m^{-3} and:

$$R = \log_{10} \frac{Rrs_{490}}{Rrs_{555}},$$

Rrs_{490} and Rrs_{555} are the remote sensing reflectance at 490 and 555 nm, respectively, and R is called the 490-555 band ratio.

The hydrographic regions of Terra Nova Bay (TNB), Cape Adare zone (CA) and center of the Ross Gyre (RG) are among the most interesting of the Ross Sea [1]:

- the TNB polynya is the area where the high salinity shelf water (HSSW) is generated by formation and removal of ice; it is strongly affected by ice melting and nutrient release from the Drygalsky Glacier (case II waters [15]);
- the northward branch of HSSW mixes with the modified circumpolar deep water (MCDW) near CA and escapes in the northern continental shelf break;
- in RG nutrients are released into the upper ocean by water mixing processes, favoring the onset of intense phytoplankton blooms; RG is located in the Joides Basin, near the continental shelf break (case I waters [15]).

The zones under study are defined as follows (Fig. 1):

- TNB: -74.5 S – -75.25 S, 163 W – 166 W (0°.75 × 3°),
- CA: -71.5 S – -73 S, 170 W – 175 W (1°.5 × 5°),
- RG: -73.5 S – -74.5 S, 173 W – 177 W (1° × 4°).

Another interesting hydrographic region is the coastal belt from the Ross Island along the Ross Ice Shelf (RI). It has not been included because the ELF-calibration does not significantly improve the SeaWiFS Chl-a bio-optical algorithm. Nevertheless, that large polynya area is a powerful supply for the Ross Sea PP.

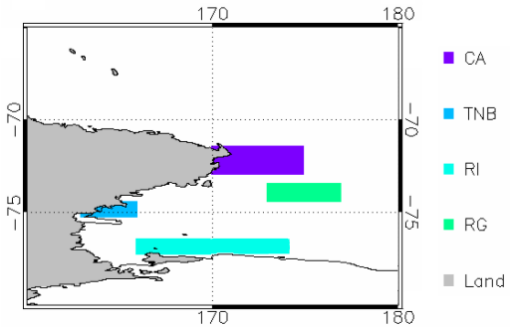

Fig. 1. Zones under study: Terra Nova Bay (TNB), Cape Adare (CA), center of the Ross Gyre (RG) and coastal belt from the Ross Island along the Ross Ice Shelf (RI).

The SeaWiFS Chl-a bio-optical algorithm has been calibrated in TNB, CA and RG with the ELF measurements of the 16th Italian Antarctic Oceanographic Campaign (January 5th 2001 – February 26th 2001). The procedure differs from that outlined above and detailed elsewhere [14] only for the calculation of the linear fit. In fact, the straight lines obtained with the standard method (least squares) or the "robust estimation" [16] do not represent well the data. This happens because almost all the experimental points (average Chl-a) lie in a symmetrical cloud and the most important of them, at least from the point of view of a linear fit (high and low Chl-a), are so few that their influence on the calculation is low (Fig. 2). For this reason a new method, the "weighted estimation" has been introduced. It can be summarized as follows:

- the center of the cloud of N experimental points (x_i, y_i) is calculated:

$$(x^*, y^*) = \left(\frac{1}{N}\sum_1^N x_i, \frac{1}{N}\sum_1^N y_i \right),$$

- the distances between the experimental points (x_i, y_i) and the center of the cloud (x^*, y^*) are computed:

$$d_i = \sqrt{(x_i - x^*)^2 + (y_i - y^*)^2},$$

- the weights:

$$w_i = d_i^2,$$

are attributed to the experimental points (x_i, y_i) before calculating the linear regression.

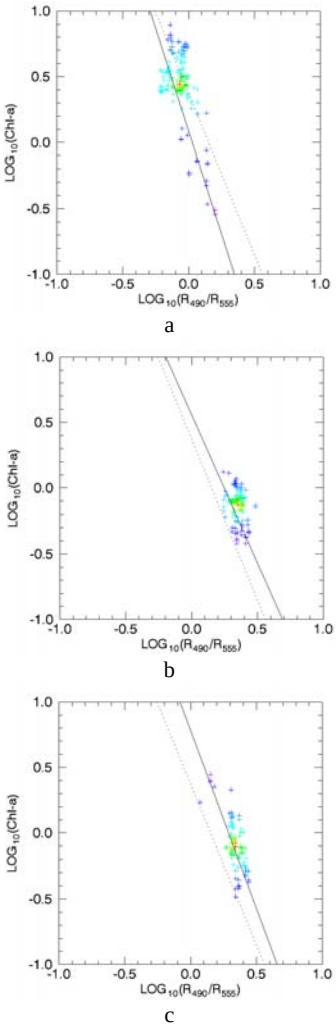

Fig. 2. ELF calibration of the SeaWiFS Chl-a bio-optical algorithm (continuous line) in: a) TNB; b) CA; c) RG. Colors correspond to the weights, from red (low) to violet (high). The dashed line represents the standard Chl-a bio-optical algorithm (OC1) [12].

The results of the ELF calibration of the SeaWiFS Chl-a bio-optical algorithm for TNB, CA and RG, as well as those obtained in a previous paper [14] for the Ross Sea Region (RSR), are resumed in Table 1 and shown in Fig. 3. RSR has been defined as the area delimited by the coast and a line, straight in the cylindrical equidistant projection, from a point near Cape Adare (72° S, 170° E) to a point near Cape Colbeck (76° S, 158° W) [14]. It has to be pointed out that RSR contains the highly productive Ross Ice Shelf polynya.

Table 1. Results of the ELF calibration of the SeaWiFS Chl-a bio-optical algorithm in TNB, CA, RG and RSR.

Zone	Number of concurrent measurements	a_0	a_1
TNB	158	0.09	-3.1
CA	126	0.56	-2.3
RG	92	0.78	-2.7
RSR	1345	0.37	-1.4

In the measurement range of the 16th Italian Antarctic Oceanographic Campaign ($-0.25 < \log_{10}(R_{490}/R_{555}) < 0.5$) our results indicate that:

- in TNB, standard OC1 overestimate Chl-a, especially at low concentrations (up to 75%),
- in CA, standard OC1 underestimate Chl-a, especially at low concentrations (up to 70%),
- in RG, standard OC1 underestimate Chl-a, especially at high concentrations (up to 50%).

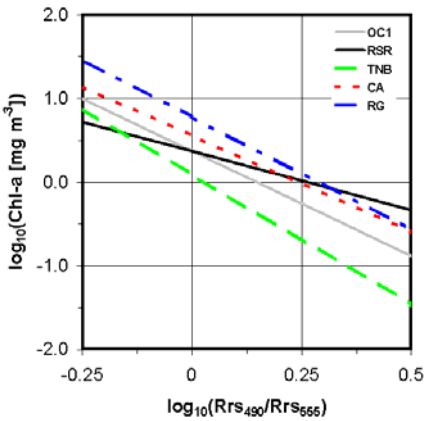

Fig. 3. Comparison among different SeaWiFS Chl-a bio-optical algorithms: OC1 (continuous gray line), ELF-calibrated during the 16th Italian Antarctic Oceanographic Campaign in RSR (continuous black line), TNB (dashed line), CA (dotted line) and RG (dot-dashed line).

As expected:

- the algorithm calibrated in CA and RG (mostly open sea and only open sea, respectively) is the

closest to OC1 (calibrated typically with measurement stations in the open sea),
- the algorithm calibrated in RSR, a sort of average algorithm of the Ross Sea, lies almost in the midst of those calibrated in TNB, CA and RG.

2.4 PP model

PP in TNB, CA and RG has been calculated with the D'-model [14]. The D'-model is a vertically generalized production model [11] calibrated in Antarctic coastal waters [17] and corrected with PAR measured by ELF during the 16th Italian Antarctic Oceanographic Campaign. PP is proportional to Chl-a in the D'-model and, as a consequence, the new PP values could differ from the standard data up to 50% – 75%.

The variables used in the D'-model are:

- C_{surf}: surface chlorophyll concentration [mgChl m^{-3}], corresponds to the Chl-a concentration measured by ELF and SeaWiFS,
- Z_{eu}: euphotic zone [m], i.e. the penetration depth of 1% surface irradiance,
- P^B_{opt}: maximum chlorophyll-specific carbon fixation rate [mgC $mgChl^{-1}$ h^{-1}], observed within a water column and measured under conditions of variable irradiance during incubations typically spanning several hours,
- D: daylength [h], also called photoperiod,
- F: relative fraction of potential photosynthesis lost within the euphotic zone due to light limitation [unitless], to first order equal to the average production of the water column divided by P^B_{opt},
- PP_{eu}: daily PP within the euphotic zone per unit of surface [mgC m^{-2} d^{-1}].

The D'-model can be summarized in the following equations:

$$PP_{eu} = P^B{}_{opt}\ F\ Z_{eu}\ C_{surf}\ D\ ,$$

$$P^B{}_{opt} = 1.09\ ,$$

$$F = 0.652\ ,$$

$$Z_{eu} = 48.8\, C_{surf}{}^{-0.36}\ .$$

For the daylength we used the formulas by Sellers [18].

3 Results and discussion

The results of the D'-model are shown in Fig. 4. In the first part of the oceanographic campaign, few radiometer data are available on TNB, CA, and RG. The available measurements show a low productivity. From the 10th day, in TNB, and from the 17th and 18th day, in RG and CA, respectively, more radiometer data are available. While the PP of CA and is about one half of that of RSR, TNB is characterized by a high PP, showing values larger than in RSR (note the peak reaching nearly 2 gC m^{-2} d^{-1} in the 33rd day). Moreover, PP decreases more slowly in TNB than in RSR.

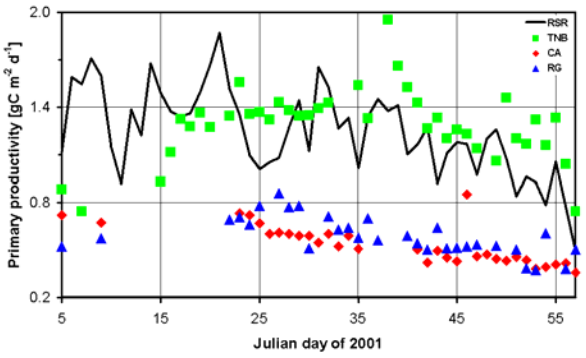

Fig. 4. PP calculated with the ELF-calibrated SeaWiFS Chl-a bio-optical algorithm in combination with the D'-model in RSR (line), TNB (squares), CA (diamonds) and RG (triangles) coming from data collected during the 16th Italian Antarctic Oceanographic Campaign.

The ELF-calibrated SeaWiFS Chl-a bio-optical algorithm and the D'-model have also been used for a new estimate of the PP in TNB, CA and RG during the Austral summers from the launch of SeaWiFS, in 1997 (Fig. 5). Looking at Fig. 5, we can observe some interesting patterns.

Firstly, the PP curve in RSR is wider for all summers. It can be higher or lower than in TNB, CA and RG because it takes into account the contributions from hydrographic regions different from those specifically under study. The maximum can be reached before or after December. In particular, the marked early bloom development in Fig. 5b and Fig. 5c can be ascribed to the Ross Ice Shelf polynya because it appears before the peak in TNB.

Secondly, TNB polynya results to be the second determining factor in PP because it strongly affects the overall behavior of RSR in summer. This effect is especially marked in January. The curves are compatible with two developing stages: earlier, in October, and later, in January, as already described in the literature [19]. The balance between the two phases depends on the season and is mainly driven by oceanographic forcings (wave motion, wind speed, sea tides and thermohaline currents) occurring in the two areas.

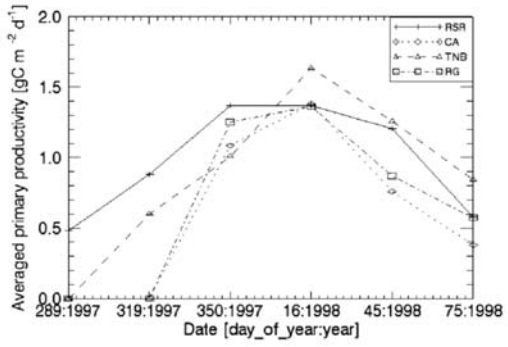

a

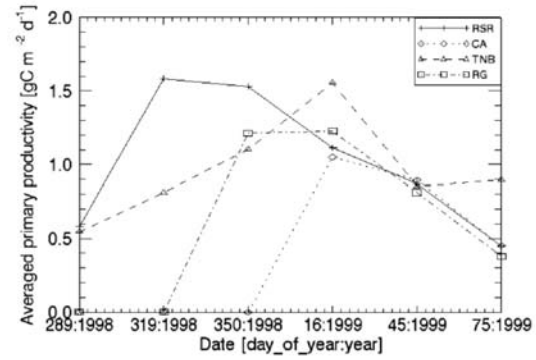

b

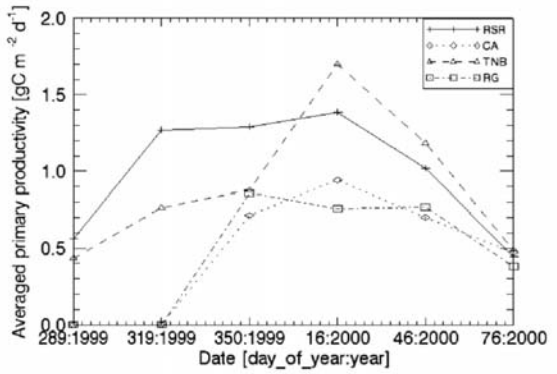

c

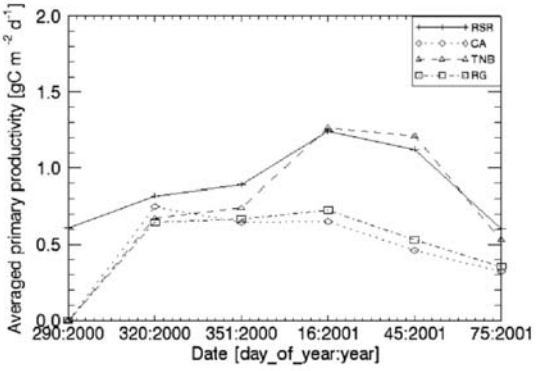

d

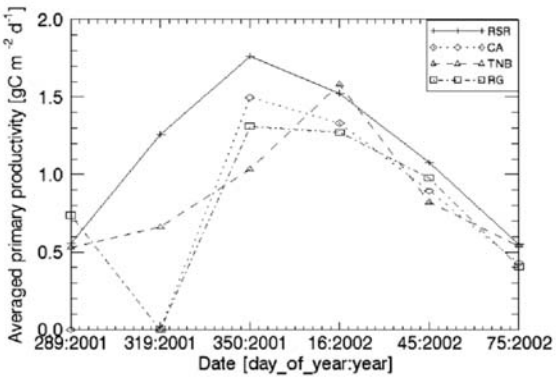

e

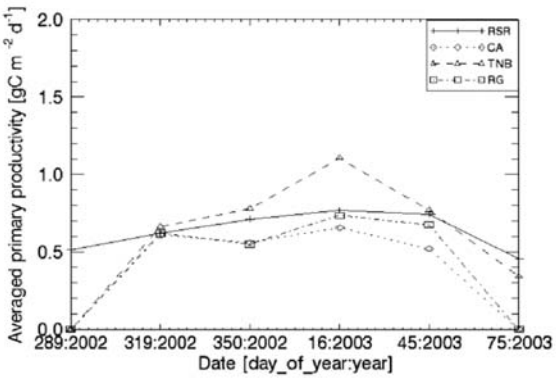

f

Fig. 5. Average PP calculated with the ELF-calibrated SeaWiFS Chl-a bio-optical algorithm in combination with the D'-model in RSR (crosses), TNB (triangles), CA (diamonds) and RG (squares) during the Austral summer: a) 1997-1998; b) 1998-1999; c) 1999-2000; d) 2000-2001; e) 2001-2002; f) 2002-2003.

Thirdly, we can observe that, in general, the phytoplankton bloom in CA and RG is weaker, begins later and is close to the maximum already before January. In both areas HSSW, characterized by high nutrient concentration and low temperature, flows in deep layers along the continental slope. Differences in seasonal productivity are mainly due to phytoplankton transport under icebergs moving from to the coastal to the offshore zone.

Eventually, looking at the sea ice concentration [20], we can conclude that primary productivity is correlated with ice coverage, at least partially: the most and the least productive summers, 2001-2002 and 2002-2003, in that order, correspond to a small and a large ice coverage of the Ross Sea, respectively.

In order to observe yearly trends, the average primary productivity in the above mentioned summers have been evaluated (Fig. 6). It is confirmed that 2001-2002 and 2002-2003 are the most and the least productive periods in CA, RG and all the Ross Sea. Also in TNB 2002-2003 is the least productive period, but the maximum PP in TNB is reached in 1998-1999. This is not surprising because TNB

is usually ice-free, and thus not sensitive to the ice coverage of the Ross Sea. In particular, it was so in all considered periods, except 2002-2003 [20]. The average PP found in this study compares well with literature data [4].

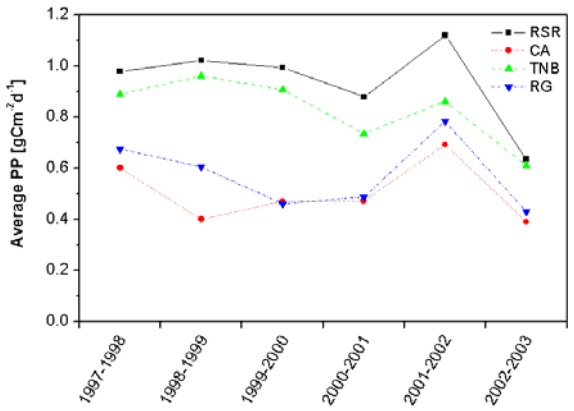

Fig. 6. Average PP calculated with the ELF-calibrated SeaWiFS Chl-a bio-optical algorithm in combination with the D'-model in RSR (squares), TNB (up-triangles), CA (circles) and RG (down-triangles) from the Austral summer 1997-1998 to the Austral summer 2002-2003.

4 Conclusion

The regional lidar calibrations of a satellite radiometer PP model in three important hydrographic provinces of the Ross Sea have been described in this report: an existing model, tuned for Antarctic waters, has been corrected with our PAR measurements and has been applied to the Chl-a concentrations obtained with an ELF-calibrated SeaWiFS bio-optical algorithm.

We found that non-local models applied to standard satellite-derived Chl-a concentrations could misestimate PP in a hydrographic province up to 50% – 75%. PP has been calculated monthly and yearly with the new models in each oceanographic region. Some relationships among phytoplankton biomass and geophysical forcings have been outlined, thus providing more insight into the complex structure of the ecological interrelations. The PP values we have obtained compare well with those independently found by other authors.

Two important conclusions can be drawn from this study. From one hand, it is confirmed that we still need optoelectronics instruments measuring Chl-a in close proximity to the sea, especially if, like ELF, they are able to operate H24. From the other hand, it is demonstrated how useful can be a regional calibration of Chl-a algorithms and PP models in order to obtain an accurate estimate of oceanic phytoplankton.

Acknowledgements

We are deeply indebted to R. Barbini and R. Fantoni for constant encouragements.

This work has been supported by PNRA – Technology Sector, 5b1 and 11-5 Projects, PRNA – Oceanographic Sector, 8.3 Project and by an ENEA fellowship (Igor G. Okladnikov).

The authors would like to thank the SeaWiFS Project (Code 970.2) and the Distributed Active Archive Center (Code 902) at the Goddard Space Flight Center, Greenbelt, MD 20771, for the production and distribution of these data, respectively. These activities are sponsored by NASA's Mission to Planet Earth Program.

References

[1] G. Budillon, M. Pacciaroni, S. Cozzi, P. Rivaro, G. Catalano, C. Ianni, C. Cantoni, , Antarctic Science **15**, 105 (2003).

[2] P. W. Boyd, Journal of Phycology, **38**, 844 (2002).

[3] S. Alvain, C. Moulin, H. Loisel, Y. Dandonneau, , 2004, Improved SeaWiFS chlorophyll a estimates using a species dependent bio-optical model for case I waters (OC4-SD), in E-proceedings of Ocean Optics XVII, edited by S. Ackleson (Fremantle: ONR).

[4] K. R. Arrigo, D. Worthen, A. Schnell, M. P. Lizotte, Journal of Geophysical Research C, **103**, 15587 (1998).

[5] S. B. Hooker, W. E. Esaias, G. C. Feldman, W. W. Gregg, McClain, C. R., 1992, An overview of SeaWiFS and ocean color, in SeaWiFS Technical Report Series, NASA Technical Memorandum 104566, Volume 1, edited by S. B. Hooker and E. R. Firestone (Greenbelt: NASA).

[6] R. Barbini, F. Colao, R. Fantoni, L. Fiorani, A. Palucci, J. Optoelectron. Adv. Mater. **3**, 817 (2001).

[7] L. Fiorani, S. Mattei, S. Vetrella, Proceedings of SPIE **3496**, 176 (1998).

[8] J. E. O'Reilly, S. Maritorena, M. C. O'Brien, D. A. Siegel, D. Toole, D. Menzies, R. C. Smith, J. L. Mueller, B. Greg Mitchell, M. Kahru, F. P. Chavez, P. Strutton, G. F. Cota, S. B. Hooker, C. R. McClain, K. L. Carder, F. Müller-Karger, L. Harding, A. Magnuson, D. Phinney, G. F. Moore, J. Aiken, K. R. Arrigo, R. Letelier, M. Culver, 2000, SeaWiFS Postlaunch Calibration and Validation Analyses, Part 3, in SeaWiFS Postlaunch Technical Report Series, NASA Technical Memorandum 2000-206892, Volume 11, edited by S. B. Hooker and E. R. Firestone (Greenbelt: NASA).

[9] C. R. McClain, G. C. Feldman, S. B. Hooker, Deep-Sea Research II **51**, 5 (2004).

[10] R. Barbini, F. Colao, L. De Dominicis, R. Fantoni, L. Fiorani, A. Palucci, E. S. Artamonov, International Journal of Remote Sensing **25**, 2095 (2004).

[11] M. J. Behrenfeld, P. G. Falkowski, Limnology and

Oceanography **42**, 1479 (1997).
[12] J. E. O'Reilly, S. Maritorena, B. G. Mitchell, D. A. Siegel, K. L. Carder, S. A. Garver, M. Kahru, C. McClain, Journal of Geophysical Research C **103**, 24937 (1998).
[13] R. Barbini, F. Colao, R. Fantoni, L. Fiorani, A. Palucci, International Journal of Remote Sensing **24**, 3205 (2003).
[14] F.Colao, R. Fantoni, L. Fiorani, A. Palucci, I. G. Okladnikov, J. Optoelectron. Adv. Mater. **7**, 1091 (2005).
[15] International ocean-colour coordinating group, 2000, Remote Sensing of Ocean Colour in Coastal, and Other Optically-complex, Waters (Dartmouth: IOCCG).
[16] W. H. Press, S. A. Teukolsky, W. T. Vetterling, B. P. Flannery, 1992, Numerical Recipes in C (Cambridge: Cambridge University Press).
[17] H. M. Dierssen, M. Vernet, R. C. Smith, Antarctic Science **12**, 20 (2000).
[18] W. D. Sellers, Physical Climatology, University of Chicago Press, Chicago, US (1965).
[19] L. Lazzara, V. Saggiomo, M. Innamorati, O. Mangoni, L. Massi, G. Mori, C. Nuccio, 2000, Photosynthetic parameters, irradiance and production estimates in the western Ross Sea, in Ross Sea Ecology. Italiantartide Expeditions (1987-1995), pp. 259-273, edited by F. Faranda, L. Guglielmo and A. Ianora (Berlin, Springer-Verlag).
[20] D. Cavalieri, P. Gloerson, J. Zwally, 2003, DMSP SSM/I Daily Polar Gridded Sea Ice Concentrations, edited by J. Maslanik and J. Stroeve (Boulder: NSIDC).

*Corresponding author: fiorani@frascati.enea.it